metals

MDPI

Article

Improved Anti-Saturation Performance of Fe-Si-Al Soft Magnetic Powder Core via Adjusting the Alloy Composition

Bowei Zhang [1], Zhongqiu Zou [1], Xuebin Zhang [1,*], Yu Han [2,*], Wei Liu [1] and Hailin Su [1,*]

[1] Anhui Red Magneto-Electric Technology Co., Ltd., Wuhu 241002, China; zhangbowei@red-mag.com.cn (B.Z.); zouzhg@red-mag.com.cn (Z.Z.); weiliu@hfut.edu.cn (W.L.)
[2] State Key Laboratory of Advanced Power Transmission Technology, State Grid Smart Grid Research Institute Co., Ltd., Beijing 102211, China
* Correspondence: zhxb@hfut.edu.cn (X.Z.); epri313@sina.com (Y.H.); hailinsu@hfut.edu.cn (H.S.)

Abstract: Ball-milled Fe-Si-Al soft magnetic powder cores with the particle compositions away from the classical Sendust point were prepared in this work. The influences of alloy composition on the metallographic structure, density, hardness, and resistivity of Fe-Si-Al alloy, as well as the frequency-dependent permeability, loss, and the anti-saturation performance of Fe-Si-Al powder cores, were investigated systematically. It was found that the hardness of Fe-Si-Al alloy increases with the Si mass ratio and the saturation magnetization (M_s) increases with the Fe mass ratio. The alloy hardness affects the particle size after the ball-milling process and, thus, influences the porosity of the powder core. Together with adjusting the demagnetization field by controlling the particle size and the core's porosity, changing the alloy composition to drive K and λ deviating from zero can effectively improve the anti-saturation performance of Fe-Si-Al powder cores at the expense of hysteresis loss, to some extent. In this work, good comprehensive magnetic properties were obtained in the $Fe_{85.5}$-Si_{12}-$Al_{2.5}$ powder core. Its effective permeability percentage at 100 Oe and M_s were 59.12% and 132.23 emu/g, respectively, which are higher than those of the classical Sendust core. This work provides a feasible idea for optimizing the overall performance of the high-power magnetic device.

Keywords: Fe-Si-Al soft magnetic powder core; alloy composition; porosity; anti-saturation performance; saturation magnetization

Citation: Zhang, B.; Zou, Z.; Zhang, X.; Han, Y.; Liu, W.; Su, H. Improved Anti-Saturation Performance of Fe-Si-Al Soft Magnetic Powder Core via Adjusting the Alloy Composition. *Metals* **2024**, *14*, 107. https://doi.org/10.3390/met14010107

Academic Editor: Imre Bakonyi

Received: 13 October 2023
Revised: 1 January 2024
Accepted: 4 January 2024
Published: 16 January 2024

1. Introduction

With the increase of both the power and switching frequency of electronic devices, soft magnetic powder cores, as a new type of magnetic composite composed of numerous distributed air gaps and high-quality insulated magnetic particles, have gained more and more attention in recent years. In addition to permeability, core loss, and saturation magnetization, which are important for traditional soft magnetic materials (such as silicon steel, ferrite, and amorphous alloy), anti-saturation performance, which can be evaluated by the percentage of permeability that can be retained with the increase of the applied magnetic field, is also a key parameter for powder cores [1–5]. It directly determines the load inductance of the powder-core-based inductor and affects the winding turns and the ripple percentage in the winding, which poses significant effects on the copper loss of the inductor [6]. Consequently, for some high-power applications where the inductor's copper loss is higher than the iron loss, the anti-saturation performance of the powder core is even more important than its permeability and core loss [7,8].

The anti-saturation performance of powder cores is mainly related to the demagnetization field of powder cores and the resistance to magnetic moment rotation. The demagnetization field of the powder core affects the magnitude of the magnetic field loaded on each magnetic particle. The larger the demagnetization field, the smaller the actual magnetic field loaded on the powder particles, and the better the anti-saturation performance of the powder core [9]. The demagnetization field is mainly composed of the structural

demagnetization field between magnetic particles and the internal demagnetization field within each particle [10,11]. The structural demagnetization field, generally reflected by the powder core's density, is related to the volume fraction of non-magnetic materials, including insulation substance and air gaps between different magnetic particles [12]. The more non-magnetic materials, the larger the field of structural demagnetization. The internal demagnetization field is mainly related to the particle size. The smaller the particle size, the larger the internal demagnetization field. At present, researchers have improved the anti-saturation performance of powder cores by increasing the thickness of the magnetic particle insulation layer, decreasing the density of the core, and increasing the proportion of fine powder to increase both the structural and internal demagnetization fields within the core. In detail, increasing the insulating layer thickness would enlarge the distributed air gaps, thus improving the structural demagnetization field and anti-saturation performance of the powder core. However, this would inevitably lead to a decrease in permeability. For example, some researchers investigated the effect of an insulation material's content on the magnetic properties of Fe-Si-Al powder cores, and they found that the percentages of effective permeability at 100 Oe would increase approximately from 40% to 75% as the insulation material's content increased from 3 wt.% to 11 wt.%, while in the meantime, the permeability level was reduced from 75 μ to 45 μ [13,14]. As mentioned above, a suitable particle size ratio would optimize the anti-saturation performance of powder cores, which has already been adopted by some researchers to improve the anti-saturation performance of Fe-Si-Al powder cores. To be concrete, the researchers found that the percentages of effective permeability of Fe-Si-Al powder cores at 100 Oe slightly increased from 50% to 53% when the proportion of Fe-Si-Al fine powder increased from 15% to 35% [15]. Nevertheless, a side effect, usually the deterioration of permeability and saturation magnetization, was also induced by these methods [16–18]. Another method of improving the anti-saturation performance of the powder core is to enhance the magneto-crystalline anisotropy and magnetostriction of magnetic particles by changing the powder's composition to make the magnetic moments within each particle more difficult to rotate. Although this method inevitably increases the hysteresis loss of the core, the total loss of the inductors can be decreased due to the decrease of the winding's copper loss in some high-power applications, as mentioned above. In many high-power inductors, copper loss is the main loss, making it a feasible method to change the powder's composition and sacrifice iron loss to improve the anti-saturation performance.

Generally, the composition of the alloy determines its comprehensive properties. For instance, when the Ti content in Fe-Si-Al increased from 0% to 2.5%, the saturation magnetization of Fe-Si-Al-Ti gradually decreased. In contrast, the addition of Ni element made the saturation magnetization of Fe-Si-Ni alloy reach 254.4 emu/g. Briefly, it holds great potential to optimize the alloy's overall properties by changing the composition [19–24]. Fe_{85}-$Si_{9.6}$-$Al_{5.4}$, as the composition of Sendust alloy, possesses a near-zero magneto-crystalline anisotropy constant, a zero magnetostriction coefficient, and high resistivity. These advantages result in low hysteresis loss, low eddy current loss, and good frequency stability of high permeability, making Fe-Si-Al the most widely used powder core [25–27]. However, the very composition also causes a weak anti-saturation capability and low saturation magnetization, which leads to the problem of low anti-saturation performance and the large volume of the Fe-Si-Al powder core. Accordingly, in this work, the anti-saturation performance of the Fe-Si-Al powder core was optimized through adjusting the alloy composition of Fe-Si-Al particles, with special emphasis on the magneto-crystal anisotropy constant (K) and the magnetostriction coefficient (λ). It was found that adjusting the alloy composition of Fe-Si-Al particles away from the point, when K and λ are equal to zero, can effectively improve the anti-saturation performance of corresponding powder cores. In addition, when the percentages of Si and Al in Fe-Si-Al are maintained at a low level, the Fe-Si-Al alloy achieves high-saturation magnetization. This paper provides fresh ideas and valuable reference for improving the anti-saturation performance and saturation magnetization of Fe-Si-Al soft magnetic powder cores and lays the foundation for the application of Fe-Si-Al powder cores in high-power devices.

2. Experimental

2.1. Alloy Composition Selection

Figure 1 shows the classic ternary diagram of Fe-Si-Al alloy, in which three curves can be seen: curve 1 for composition with K equals zero, curve 2 for composition with λ equals zero, and curve 3 for composition with the highest permeability. The Fe_{85}-$Si_{9.6}$-$Al_{5.4}$ composition point (Sendust) is near the intersection of the three curves. It leads to high permeability and low loss for the Fe-Si-Al alloy and, thus, is selected as the very composition of most Fe-Si-Al powder cores. In this experiment, six composition points with different K and λ (marked in red in Figure 1) were selected, and the corresponding master alloys have been prepared to investigate the influence of composition on the physical properties of Fe-Si-Al powder cores. In detail, the six samples and their magnetic characteristics are summarized in Table 1.

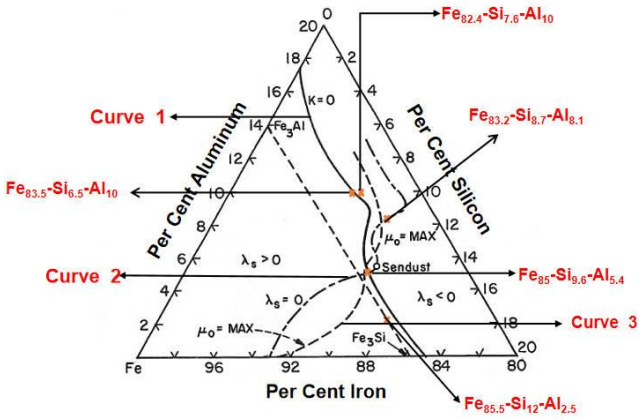

Figure 1. Ternary diagram of Fe-Si-Al alloy (Reprinted/Adapted from Ref. [28]).

Table 1. Magnetic characteristics of selected compositions of Fe-Si-Al alloy.

Composition	K	λ
$Fe_{82.4}$-$Si_{7.6}$-Al_{10}	≈0	>0
$Fe_{83.2}$-$Si_{8.7}$-$Al_{8.1}$	≠0	=0
$Fe_{83.5}$-$Si_{6.5}$-Al_{10}	=0	>0
Fe_{85}-$Si_{9.6}$-$Al_{5.4}$	≈0	=0
$Fe_{85.5}$-Si_{12}-$Al_{2.5}$	≈0	<0
$Fe_{87.1}$-$Si_{9.9}$-Al_3	≠0	<0

2.2. Preparation of Master Alloys and Powders

Firstly, high-purity iron, silicon, and aluminum ingots were melted and casted to form the alloy in a medium-frequency induction heating furnace under an air atmosphere. By adjusting the mass ratio of iron, silicon, and aluminum, six alloys with the compositions of $Fe_{82.4}$-$Si_{7.6}$-Al_{10}, $Fe_{83.2}$-$Si_{8.7}$-$Al_{8.1}$, $Fe_{83.5}$-$Si_{6.5}$-Al_{10}, Fe_{85}-$Si_{9.6}$-$Al_{5.4}$, $Fe_{85.5}$-Si_{12}-$Al_{2.5}$, and $Fe_{87.1}$-$Si_{9.9}$-Al_3 were obtained, respectively. Then, these Fe-Si-Al alloys were coarsely broken, and ball-milled into powders. For ball milling, the ball to powder mass ratio was 8:1, the powder to ethanol mass ratio was 1:1, and the ball milling time was 6 h. The prepared magnetic powders were dried at 60 °C and finally annealed at 640 °C under a nitrogen atmosphere for 90 min.

2.3. Preparation of Soft Magnetic Powder Cores

A certain content of aqueous phosphoric acid solution was mixed with magnetic powder at 120 °C until the water completely evaporated. Then, the dried magnetic powders were evenly mixed with 4 wt.‰ of zinc stearate and resin powder, and the mixture was sieved by an 80-mesh sieve to remove large particles. The sieved powder was then pressed into rings with an outer diameter of 26.9 mm, an inner diameter of 14.7 mm, and a height of 11.2 mm at a pressure of 1860 MPa. Finally, the rings were annealed at 760 °C for 40 min under a nitrogen atmosphere.

2.4. Characterization

The X-ray diffraction (XRD) measurement was performed on a PANalytical X'pert PRO diffractometer (PANalytical, Almelo, The Netherlands) with Cu-Kα radiation to determine the sample's phase composition and crystalline structure. The metallographic structure of the alloy was observed by a metallographic microscope (Dingpa Meta-X3DA) (Dingpa Precision Instrument (Shenzhen) Co., Ltd., Shenzhen, China). A field-emission scanning electron microscope (FE-SEM, Regulus 8230) (Hitachi Ltd., Tokyo, Japan) equipped with an energy dispersive spectroscopy was employed to investigate the morphology and element distribution state. The elemental composition of Fe-Si-Al alloys was measured using an XRF analyzer (EDX4500H) (Jiangsu Skyray Instrument Co., Ltd., Kunshan, China). The Fe-Si-Al powder core should first be dipped in wax and then the density can be obtained by the drainage method. The ratio of the density of the Fe-Si-Al powder core to the density of Fe-Si-Al alloy was used to characterize the porosity of the Fe-Si-Al powder core. The alloy hardness was measured by a Rockwell hardness tester (HR-150A) (Jinan FangYuan Testing Machine Co., Ltd., Jinan, China). A laser particle size analyzer (BT-9300S) (Bettersize Instruments Ltd., Dandong, China) was used to evaluate the particle size distribution of Fe-Si-Al powders. The static magnetic properties of the alloys were measured at room temperature using a vibrating sample magnetometer (VSM, Lakeshore 7410) (Lake Shore Cryotronics, Inc., Westerville, OH, USA). The alloy's electrical resistivity was measured using four-point probes (SevenStar D14-11D/ZM) (Beijing Sevenstar Electronics Co.,Ltd., Beijing, China). An LCR meter (Wayne Kerr 3260B) (Wayne Kerr, Bognor Regis, UK) was used to measure the core's effective permeability (μ_e) at 1 V in the frequency range of 1–2000 kHz and the anti-saturation performance in the DC magnetizing field ranging from 0 Oe to 200 Oe under the condition of 100 kHz/1 V. The *B-H* analyzer (IWATSU 8218) (IWATSU, Tokyo, Japan) was employed to evaluate the core loss at a frequency ranging from 100 to 800 kHz at the maximum magnetic flux density (B_m) of 20 mT. The volume resistivity of powder cores was measured by a DC resistance tester (Tonghui TH2512) (Changzhou Tonghui Electronic Co., Ltd., Changzhou, China). All these measurements were performed at room temperature.

3. Results

3.1. Composition, Microstructure, and Physical Properties of Master Alloys and Powders

Fe-Si-Al alloys with different compositions were prepared through the melting process. In order to ensure that no compositional segregation of Fe-Si-Al alloys occurred during the melting process and to ensure the accuracy of subsequent experimental data, XRF analysis was performed three times at different positions on Fe-Si-Al alloy. The data obtained are shown in Table 2. It can be seen that the master alloys' elemental compositions were very close to their corresponding feed ratios and high homogeneity was achieved in the alloy.

Table 2. Elemental compositions of Fe-Si-Al alloy.

Composition	Serial Number	Fe Content (wt.%)	Si Content (wt.%)	Al Content (wt.%)
$Fe_{82.4}$-$Si_{7.6}$-Al_{10}	1	82.35	7.63	10.02
	2	82.39	7.58	10.03
	3	82.27	7.62	10.11
$Fe_{83.2}$-$Si_{8.7}$-$Al_{8.1}$	1	83.10	8.76	8.14
	2	83.22	8.65	8.13
	3	83.21	8.72	8.07
$Fe_{83.5}$-$Si_{6.5}$-Al_{10}	1	83.34	6.56	10.10
	2	83.25	6.57	10.18
	3	83.48	6.38	10.14
Fe_{85}-$Si_{9.6}$-$Al_{5.4}$	1	84.95	9.56	5.49
	2	84.98	9.59	5.43
	3	84.94	9.62	5.44
$Fe_{85.5}$-Si_{12}-$Al_{2.5}$	1	85.29	12.13	2.58
	2	85.31	12.15	2.54
	3	85.52	11.97	2.51
$Fe_{87.1}$-$Si_{9.9}$-Al_3	1	86.96	9.91	3.13
	2	87.07	9.87	3.06
	3	86.95	9.95	3.10

Figure 2 shows metallographic diagrams of Fe-Si-Al alloys with different compositions. As can be seen from Figure 2, each master alloy with different compositions had different grain sizes under the same melting process. There was no significant correlation between the content of Fe, Si, or Al and the grain size, because the influence of composition on the grain size is extremely complex. However, there was an obvious positive relationship between hardness and Si content, as can be seen in Figure 3. The hardness of Fe-Si-Al alloy gradually increased with the increase of Si content, which was 51.5 HRC when the Si content reached 12%. In the metallurgical industry, Si is always used to enhance the strength and hardness of steel during production, but excessive silicon will reduce the plasticity and impact toughness of steel [29]. Therefore, the hardness and brittleness of the master alloy increased with the Si content, which led to the decrease of the particle size after ball milling. Particle size distribution curves of Fe-Si-Al powders with different compositions are further shown in Figure 4. On one hand, all the samples, except for $Fe_{83.5}$-$Si_{6.5}$-Al_{10} and $Fe_{85.5}$-Si_{12}-$Al_{2.5}$, had very similar particle size distributions, with D_{50} sizes around 25 μm. Thus, the influences of particle size distribution should be the same for these samples. On the other hand, the D_{50} sizes of $Fe_{83.5}$-$Si_{6.5}$-Al_{10} and $Fe_{85.5}$-Si_{12}-$Al_{2.5}$ were 30.76 μm and 22.76 μm, respectively, confirming the influence of Si content on the hardness and brittleness. Generally, the particle size distribution of the powder will have an effect on the density and porosity of the Fe-Si-Al powder cores. Powders with a large particle size usually have better fluidity, and it is easy to obtain a high density and low porosity during the powder-pressing process. However, considering similar particle size distributions in this case, the density and porosity of the powder core samples should be largely influenced by other parameters.

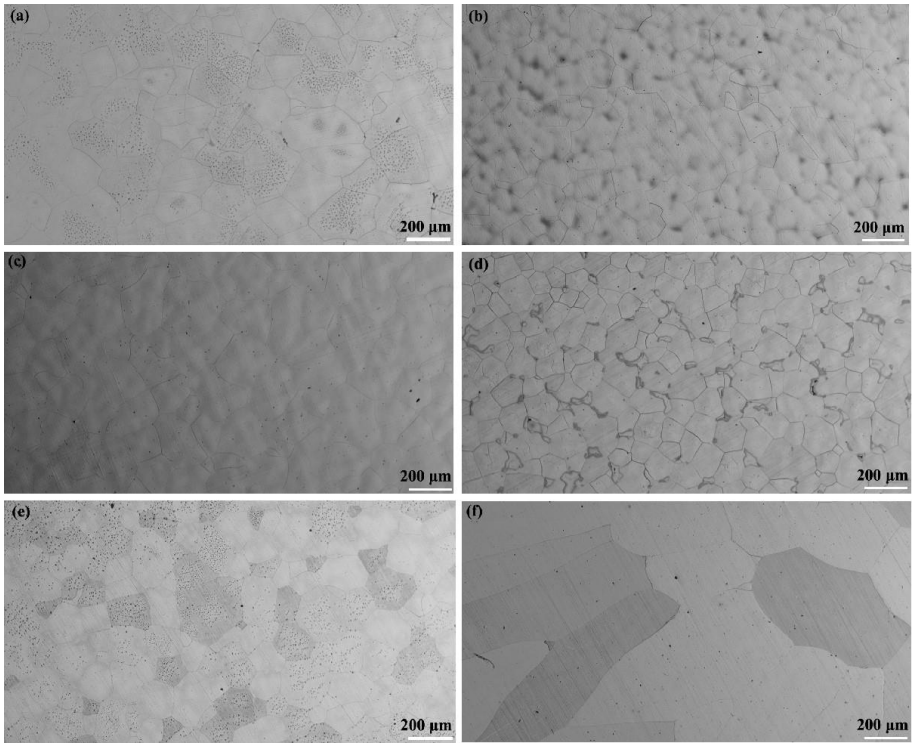

Figure 2. Metallography of (**a**) $Fe_{82.4}$-$Si_{7.6}$-Al_{10}, (**b**) $Fe_{83.2}$-$Si_{8.7}$-$Al_{8.1}$, (**c**) $Fe_{83.5}$-$Si_{6.5}$-Al_{10}, (**d**) Fe_{85}-$Si_{9.6}$-$Al_{5.4}$, (**e**) $Fe_{85.5}$-Si_{12}-$Al_{2.5}$, and (**f**) $Fe_{87.1}$-$Si_{9.9}$-Al_3 alloys.

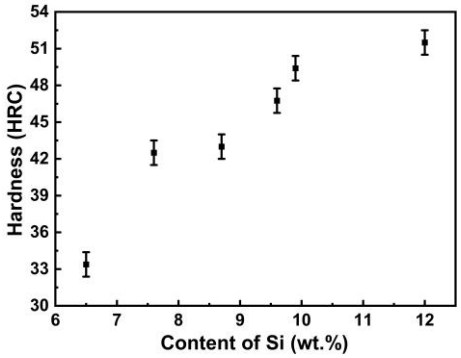

Figure 3. Dependence of the hardness of Fe-Si-Al alloy on the Si content.

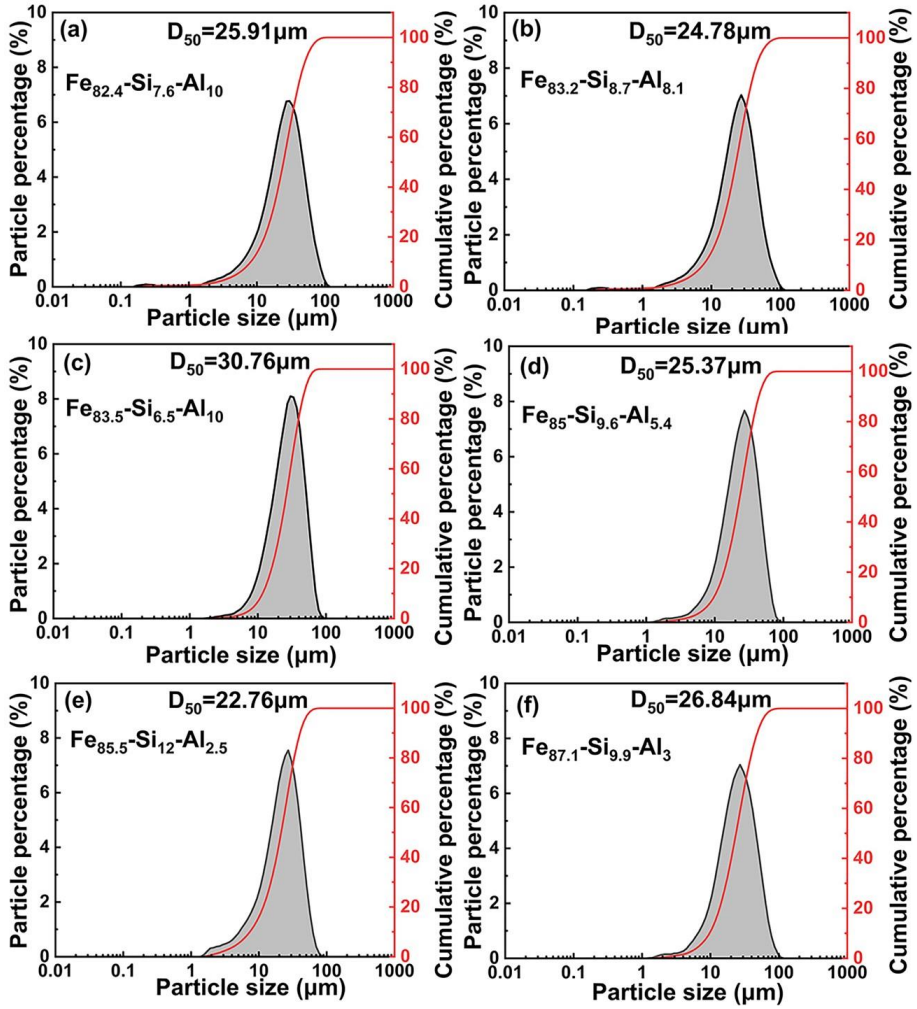

Figure 4. Particle size distribution curves of (**a**) $Fe_{82.4}$-$Si_{7.6}$-Al_{10}, (**b**) $Fe_{83.2}$-$Si_{8.7}$-$Al_{8.1}$, (**c**) $Fe_{83.5}$-$Si_{6.5}$-Al_{10}, (**d**) Fe_{85}-$Si_{9.6}$-$Al_{5.4}$, (**e**) $Fe_{85.5}$-Si_{12}-$Al_{2.5}$, and (**f**) $Fe_{87.1}$-$Si_{9.9}$-Al_3.

Table 3 shows the resistivity and density of Fe-Si-Al alloys with different compositions. The resistivity of Fe-Si-Al alloys does not have a simple relation with the composition, owing to the fact that the alloys' resistivity is affected by a variety of factors, including the composition and grain size [30]. As for Fe-Si-Al alloys, the solute Si and Al atoms dissolved in the Fe lattice to form a solid solution, leading to the change in the lattice constants of Fe and the generation of lattice distortion. Consequently, the probability of electron scattering increased, endowing the alloy with a high resistivity. Different contents of Si and Al atoms would also cause different resistivities. Besides, Fe-Si-Al alloy's grain size would also have an

impact on its resistivity. When the grain size is large, the number of internal grain boundaries is small. Therefore, the transportation of electrons is less affected, resulting in lower resistivity. Considering the coexistence of different factors, it is hard to illustrate the influences of alloys' compositions on their resistivities. The alloy density is basically determined by the mass ratio of Fe, Si, and Al. Thus, $Fe_{87.1}$-$Si_{9.9}$-Al_3 and $Fe_{82.4}$-$Si_{7.6}$-Al_{10} alloys with the relatively highest and lowest Fe content have the highest and lowest density, respectively.

Table 3. Resistivity and density of Fe-Si-Al alloys with different compositions.

Composition	Resistivity (Ω·m)	Density (g/cm^3)
$Fe_{82.4}$-$Si_{7.6}$-Al_{10}	3.4×10^{-7}	5.60
$Fe_{83.2}$-$Si_{8.7}$-$Al_{8.1}$	6.7×10^{-7}	6.94
$Fe_{83.5}$-$Si_{6.5}$-Al_{10}	4.6×10^{-7}	5.73
Fe_{85}-$Si_{9.6}$-$Al_{5.4}$	6.1×10^{-7}	6.95
$Fe_{85.5}$-Si_{12}-$Al_{2.5}$	3.0×10^{-7}	6.29
$Fe_{87.1}$-$Si_{9.9}$-Al_3	5.5×10^{-7}	7.15

Figure 5 shows the *M*-*H* hysteresis loops of Fe-Si-Al alloys with different compositions. Narrow loops, reflecting low coercivity, indicate good soft magnetic properties of all alloys. The slope of the magnetization curve of Fe_{85}-$Si_{9.6}$-$Al_{5.4}$ alloy is slightly higher than that of the other five alloys with different compositions. This indicates that large deviation of K or λ from zero increases the difficulty of the magnetization process, which helps to improve the alloy's anti-saturation capability. Table 4 displays saturation magnetizations and coercivities of Fe-Si-Al alloys with different compositions. Clearly, increasing the Fe content enhanced M_s. The saturation magnetization of Fe-Si-Al alloy increased from 65 emu/g to 141.3 emu/g as the Fe content increased from 82.4 wt.% to 87.1 wt.%. This is because Si and Al are non-magnetic substances, and when the ratio of the two elements decreased, the saturation magnetization of Fe-Si-Al alloy increased. This led to M_s values of 141.3 emu/g and 132.23 emu/g for $Fe_{87.1}$-$Si_{9.9}$-Al_3 and $Fe_{85.5}$-Si_{12}-$Al_{2.5}$ alloys, respectively, which are 11% and 4% higher than Fe_{85}-$Si_{9.6}$-$Al_{5.4}$ alloy, respectively. This may contribute to a higher operating magnetic flux density in magnetic devices, which can reduce the consumption of both the core and the winding, thereby reducing the total loss and cost of magnetic devices. In addition, Fe-Si-Al alloys are soft magnetic materials and have low coercivity, which can also be seen in Table 4. It is worth noting that $Fe_{83.5}$-$Si_{6.5}$-Al_{10} with K equal to 0 had the lowest coercivity, at 124.8 A/m.

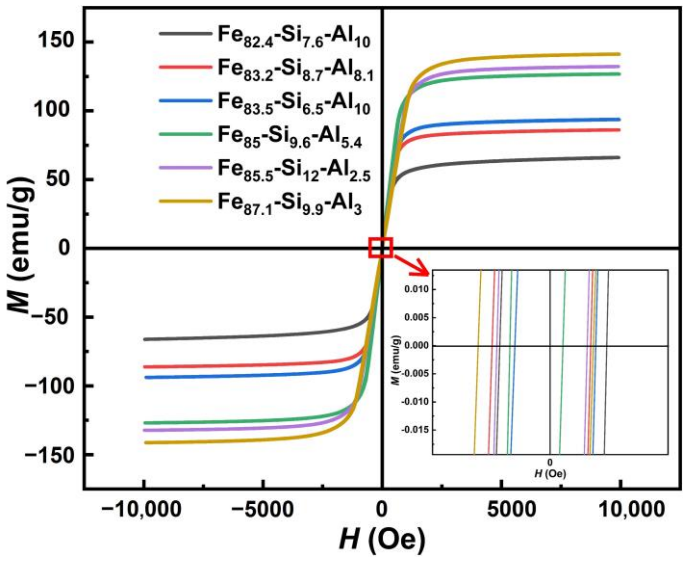

Figure 5. *M*-*H* hysteresis loops of Fe-Si-Al alloys with different compositions.

Table 4. Saturation magnetizations and coercivities of Fe-Si-Al alloys with different compositions.

Composition	Saturation Magnetization (emu/g)	Coercivity (A/m)
$Fe_{82.4}$-$Si_{7.6}$-Al_{10}	66.12	178.4
$Fe_{83.2}$-$Si_{8.7}$-$Al_{8.1}$	86.20	176.0
$Fe_{83.5}$-$Si_{6.5}$-Al_{10}	93.66	124.8
Fe_{85}-$Si_{9.6}$-$Al_{5.4}$	126.90	174.4
$Fe_{85.5}$-Si_{12}-$Al_{2.5}$	132.23	234.4
$Fe_{87.1}$-$Si_{9.9}$-Al_3	141.30	215.2

Figure 6 exhibits XRD patterns of various ball-milled Fe-Si-Al powders after annealing. Three prominent diffraction peaks can be recognized, which should be associated with (220), (400), and (422) planes of cubic α-Fe(Si, Al) solid solution. No significant difference in phase composition could be identified from the XRD patterns, indicating that the alloy formed by melting was Fe-Si-Al alloy and ball milling did not change the phase composition. The grain size of Fe-Si-Al powders with different compositions was calculated by the Debye–Scherrer equation, which is expressed as:

$$D_{\mathrm{HKL}} = \frac{K\lambda}{\beta_{\mathrm{HKL}} cos\theta_{\mathrm{HKL}}} \quad (1)$$

where D_{HKL} is the average thickness of the grain in the direction normal to the (HKL) crystal plane, λ is the wavelength of the X-rays used, and its value is 0.154056 nm, θ_{HKL} is the Bragg angle of the (HKL) crystal plane diffraction, and β_{HKL} is the linewidth of the (HKL) crystal plane diffraction, which can be defined as half-height width, or integral width. K is a constant with a value of 0.89 when β is defined as half-height width. Table 5 shows the grain size of Fe-Si-Al powders with different compositions. Owing to the same processing conditions, Fe-Si-Al powders with different compositions had very similar grain sizes, around 30 nm. Therefore, the influence of grain size on the overall properties of the powder core samples can be neglected to some extent.

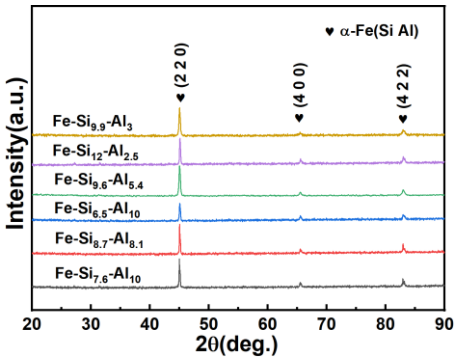

Figure 6. XRD patterns of ball-milled Fe-Si-Al powders with different compositions after annealing.

Table 5. The grain sizes of Fe-Si-Al powders with different compositions.

Composition	Grain Size (nm)
$Fe_{82.4}$-$Si_{7.6}$-Al_{10}	30.35
$Fe_{83.2}$-$Si_{8.7}$-$Al_{8.1}$	28.83
$Fe_{83.5}$-$Si_{6.5}$-Al_{10}	31.60
Fe_{85}-$Si_{9.6}$-$Al_{5.4}$	32.11
$Fe_{85.5}$-Si_{12}-$Al_{2.5}$	30.41
$Fe_{87.1}$-$Si_{9.9}$-Al_3	31.26

3.2. Physical Properties of Powder Cores

Table 6 shows the resistivity of Fe-Si-Al powder cores with different compositions. Compared to the corresponding master alloys, the resistivities of the powder cores were

significantly improved, demonstrating good insulation quality for all samples. With the increase of Fe content in the alloy, resistivity showed a decreasing trend after an initial increase. It is documented that the composition of the magnetic powder, the quality and thickness of the insulating layer, and the porosity of the powder core can affect the resistivity of powder cores. Considering the giant increase in resistivity from master alloys to powder cores, the insulating layer and the porosity should dominate the resistivity. However, we should mention that alloys' compositions have a certain effect on the insulating layer and the porosity in this case. For instance, Figure 7 shows SEM images of polished cross-sections of powder core samples. The thicknesses of the insulating layers for $Fe_{82.4}$-$Si_{7.6}$-Al_{10}, $Fe_{83.2}$-$Si_{8.7}$-$Al_{8.1}$, $Fe_{83.5}$-$Si_{6.5}$-Al_{10}, Fe_{85}-$Si_{9.6}$-$Al_{5.4}$, $Fe_{85.5}$-Si_{12}-$Al_{2.5}$, and $Fe_{87.1}$-$Si_{9.9}$-Al_3 were 2.7, 4.0, 3.5, 2.17, 2.16, and 1.70 μm, respectively. It can be inferred that Fe-Si-Al alloy powders with different compositions have different corrosion resistances, resulting in different thicknesses of their insulation layers after the same insulating process. In addition to the thickness, the roughness of the insulating layers should also be different. Thus, in the pressing process, there will be differences in the density and porosity of the Fe-Si-Al powder cores, due to the change in the fluidity of the insulated powders.

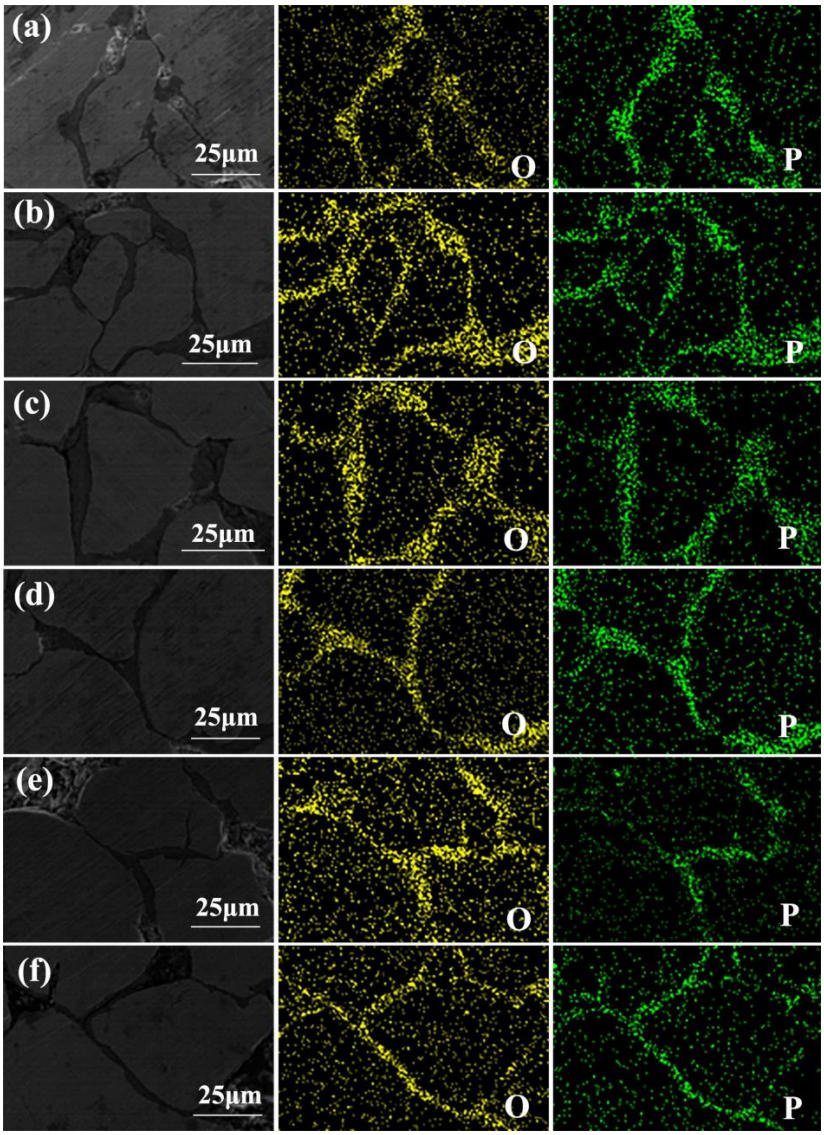

Figure 7. SEM images of the cross-section and corresponding element distribution (O and P elements) of (**a**) $Fe_{82.4}$-$Si_{7.6}$-Al_{10}, (**b**) $Fe_{83.2}$-$Si_{8.7}$-$Al_{8.1}$, (**c**) $Fe_{83.5}$-$Si_{6.5}$-Al_{10}, (**d**) Fe_{85}-$Si_{9.6}$-$Al_{5.4}$, (**e**) $Fe_{85.5}$-Si_{12}-$Al_{2.5}$, and (**f**) $Fe_{87.1}$-$Si_{9.9}$-Al_3 powder cores.

Table 6. Resistivity of Fe-Si-Al powder cores with different alloy compositions.

Composition	Resistivity (Ω·m)
$Fe_{82.4}$-$Si_{7.6}$-Al_{10}	0.159
$Fe_{83.2}$-$Si_{8.7}$-$Al_{8.1}$	0.324
$Fe_{83.5}$-$Si_{6.5}$-Al_{10}	0.136
Fe_{85}-$Si_{9.6}$-$Al_{5.4}$	6.260
$Fe_{85.5}$-Si_{12}-$Al_{2.5}$	3.170
$Fe_{87.1}$-$Si_{9.9}$-Al_3	0.383

Table 7. Density and porosity of Fe-Si-Al powder cores with different compositions.

Composition	Density (g/cm^3)	Porosity (%)
$Fe_{82.4}$-$Si_{7.6}$-Al_{10}	5.11	9
$Fe_{83.2}$-$Si_{8.7}$-$Al_{8.1}$	5.34	23
$Fe_{83.5}$-$Si_{6.5}$-Al_{10}	5.35	7
Fe_{85}-$Si_{9.6}$-$Al_{5.4}$	5.49	21
$Fe_{85.5}$-Si_{12}-$Al_{2.5}$	5.38	14
$Fe_{87.1}$-$Si_{9.9}$-Al_3	5.38	25

Figure 8 shows the effective permeability of Fe-Si-Al powder cores with different compositions. Compared to those prepared with particles of the same composition, powder cores with different alloy compositions presented a permeability variation tendency totally different from that of the core's density. This is mainly due to the difference in the anti-saturation capability of alloy particles with different compositions. Powder cores with an Fe content below 85 wt.% had a relatively high permeability. For all Fe-Si-Al powder cores with different compositions, their permeabilities were all stable with increasing frequency. This implies a low eddy current level inside these cores, which is consistent with their high resistivity shown in Table 6.

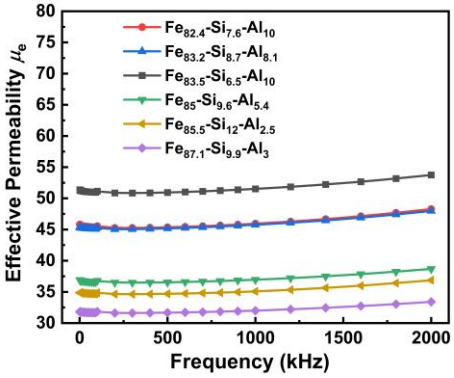

Figure 8. Frequency dependence of effective permeability of Fe-Si-Al powder cores with different compositions.

Figure 9 shows the anti-saturation performance of Fe-Si-Al powder cores with different compositions. It can be seen that the percentage of permeability of the powder core gradually decreased with the increase of the external magnetic field, due to the magnetization state of the powder core approaching saturation. Overall, powder cores with lower permeability exhibited a stronger anti-saturation capability, conforming to the law that high permeability and good anti-saturation performance can hardly be achieved simultaneously. This can be attributed to the opposite physical mechanism for these two magnetic parameters. A strong demagnetization field, high K and λ, large internal stress, and abundant defects undoubtedly make the moments in magnetic materials more difficult to rotate in the direction of the applied magnetic field [31]. This leads to poor permeability but good anti-saturation performance. For the $Fe_{87.1}$-$Si_{9.9}$-Al_3 powder core, the relatively

highest porosity, reflecting a strong structural demagnetization field within the core, and the composition of nonzero K and λ together contribute to its strongest anti-saturation capability in this work.

Compared with the Sendust powder core with the classical composition of Fe_{85}-$Si_{9.6}$-$Al_{5.4}$, the $Fe_{82.4}$-$Si_{7.6}$-Al_{10} and $Fe_{83.5}$-$Si_{6.5}$-Al_{10} cores had a higher effective permeability and lower anti-saturation performance. This may be mainly caused by the low structural demagnetization field determined by small porosity in these two cores, although the λ of their corresponding alloys was greater than zero. For the $Fe_{83.2}$-$Si_{8.7}$-$Al_{8.1}$ and $Fe_{87.1}$-$Si_{9.9}$-Al_3 cores with porosity close to the Fe_{85}-$Si_{9.6}$-$Al_{5.4}$ core, their effective permeability and anti-saturation performance were different from those of the Fe_{85}-$Si_{9.6}$-$Al_{5.4}$ core. The $Fe_{83.2}$-$Si_{8.7}$-$Al_{8.1}$ core had the highest effective permeability, followed by the Fe_{85}-$Si_{9.6}$-$Al_{5.4}$ core, and the $Fe_{87.1}$-$Si_{9.9}$-Al_3 core had the lowest effective permeability. The anti-saturation performance of the three cores exhibited an opposite variation to effective permeability. The lower passivation by phosphoric acid for the $Fe_{83.2}$-$Si_{8.7}$-$Al_{8.1}$ core with a slightly lower Fe content might make it easier to be magnetized, while the highest porosity and nonzero K and λ endow the $Fe_{87.1}$-$Si_{9.9}$-Al_3 core with the strongest resistance to magnetization. For the $Fe_{85.5}$-Si_{12}-$Al_{2.5}$ core, its porosity was lower than that of the Fe_{85}-$Si_{9.6}$-$Al_{5.4}$ core, suggesting a smaller structural demagnetization field. However, its effective permeability was lower than that of the Fe_{85}-$Si_{9.6}$-$Al_{5.4}$ core, accompanied by a better anti-saturation capability. This implies that nonzero λ and the internal demagnetization field determined by its smallest D_{50} may play a dominant role. Based on the above analysis, it can be concluded that adjusting the alloy composition deviating from the Sendust point of Fe_{85}-$Si_{9.6}$-$Al_{5.4}$ with zero K and λ while considering the particle size and the core's porosity is a feasible and effective way to improve the anti-saturation performance of Fe-Si-Al powder cores. In this work, anti-saturation properties superior to those of the Fe_{85}-$Si_{9.6}$-$Al_{5.4}$ core were achieved in $Fe_{87.1}$-$Si_{9.9}$-Al_3 and $Fe_{85.5}$-Si_{12}-$Al_{2.5}$ powder cores. At 100 Oe, the percentages of effective permeability of the $Fe_{87.1}$-$Si_{9.9}$-Al_3 and $Fe_{85.5}$-Si_{12}-$Al_{2.5}$ cores were 61.73% and 59.12%, respectively, which are higher than that of the Fe_{85}-$Si_{9.6}$-$Al_{5.4}$ core.

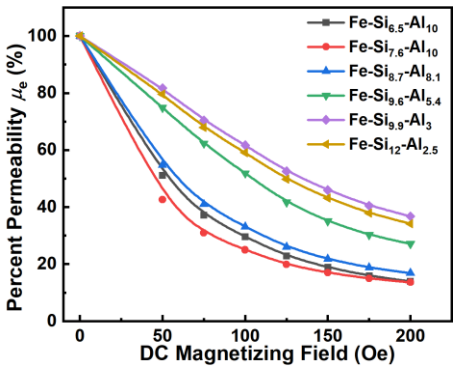

Figure 9. Percent permeability curves of Fe-Si-Al powder cores with different compositions.

Figure 10a shows the frequency dependence of core loss of Fe-Si-Al powder cores with different compositions. Apart from the loss of the $Fe_{83.2}$-$Si_{8.7}$-$Al_{8.1}$ core, the losses of the other cores were much higher than that of the Fe_{85}-$Si_{9.6}$-$Al_{5.4}$ core. To clarify the physical origin of loss deterioration for these cores, the Berttoti loss equation was used to separate core loss into hysteresis loss and eddy current loss, as shown in Figure 10b,c [32]. As is known, K and λ of magnetic particles and the demagnetization field inside the powder core determine the core's hysteresis loss, while the particle size and the core's resistivity affect the core's eddy current loss [33–35]. Obviously, a large particle size and low resistivity resulted in relatively high eddy current losses of $Fe_{83.5}$-$Si_{6.5}$-Al_{10} and $Fe_{82.4}$-$Si_{7.6}$-Al_{10} cores. The deviation of λ from zero made the magnetic moments in $Fe_{82.4}$-$Si_{7.6}$-Al_{10}, $Fe_{83.5}$-$Si_{6.5}$-Al_{10}, $Fe_{87.1}$-$Si_{9.9}$-Al_3, and $Fe_{85.5}$-Si_{12}-$Al_{2.5}$ alloys harder to rotate, resulting in hysteresis losses much higher than that of the Fe_{85}-$Si_{9.6}$-$Al_{5.4}$ core. Among these four powder cores, $Fe_{87.1}$-$Si_{9.9}$-Al_3 with K far away from zero exhibited the highest

hysteresis loss, consistent with its best anti-saturation performance. For the $Fe_{85.5}$-Si_{12}-$Al_{2.5}$ core, its lowest particle size and high resistivity led to the lowest eddy current loss and, thus, partially compensated for the increased hysteresis loss caused by the significant deviation of λ from zero. Considering the remarkable improvement in the anti-saturation capability and the moderate increase in core loss, the core with the composition of $Fe_{85.5}$-Si_{12}-$Al_{2.5}$ can be expected to realize excellent comprehensive magnetic properties in low-frequency and high-power applications.

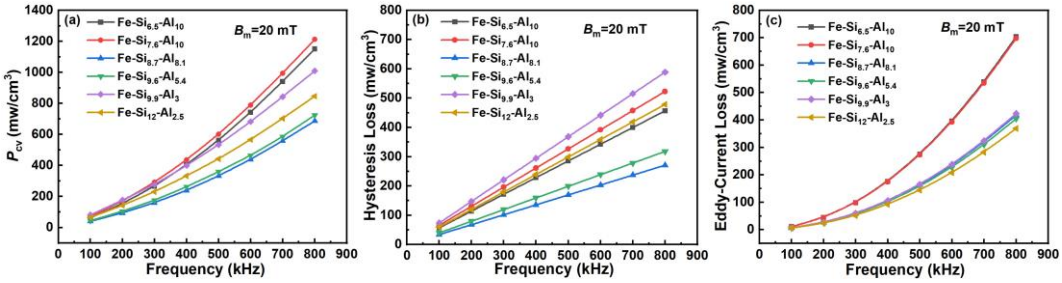

Figure 10. Frequency dependence of (**a**) core loss, (**b**) fitted hysteresis loss, and (**c**) eddy current loss for Fe-Si-Al powder cores with different compositions.

4. Conclusions

To optimize the anti-saturation performance, Fe-Si-Al alloys with different compositions, possessing different K and λ, were prepared and used to fabricate powder cores through the process of ball milling and insulating. The Fe-Si-Al alloy hardness and M_s were found to increase with the Si and Fe content, respectively. $Fe_{85.5}$-Si_{12}-$Al_{2.5}$ alloy had the relatively highest hardness of 51.5 HRC, which contributes to its smallest ball-milled particle size. $Fe_{87.1}$-$Si_{9.9}$-Al_3 and $Fe_{85.5}$-Si_{12}-$Al_{2.5}$ alloys had M_s values of 141.3 emu/g and 132.23 emu/g, which are 11% and 4% higher than that of the Fe_{85}-$Si_{9.6}$-$Al_{5.4}$ alloy, respectively. Different hardness and corrosion resistance values resulted in different particle sizes and insulation quality, which affects the powder core's porosity and, thus, determines the demagnetization field. Although effective permeability and hysteresis loss may be slightly sacrificed, anti-saturation performance can be significantly improved through increasing porosity and selecting the alloy composition with nonzero K and λ for Fe-Si-Al powder cores. Under the premise of considering effective permeability and core loss, the alloy composition of $Fe_{85.5}$-Si_{12}-$Al_{2.5}$ with good anti-saturation capability was proposed. The percentage of effective permeability at 100 Oe for the powder core with this composition was as much as 59.12% higher than that of the Fe_{85}-$Si_{9.6}$-$Al_{5.4}$ Sendust powder core. This work may shed new light on improving the anti-saturation capability and the saturation magnetization of Fe-Si-Al soft magnetic powder cores by changing the particles' composition.

Author Contributions: Conceptualization, B.Z., X.Z. and H.S.; formal analysis, B.Z. and W.L.; investigation, B.Z., X.Z., Z.Z. and Y.H.; resources, Z.Z. and H.S.; writing—original draft, B.Z.; writing—review and editing, X.Z., H.S. and W.L.; supervision, Y.H. and H.S.; funding acquisition, X.Z., Y.H. and Z.Z. All authors have read and agreed to the published version of the manuscript.

Funding: This work was supported by the Science and Technology Project of State Grid Corporation of China (No. 5500-202118252A-0-0-00).

Data Availability Statement: The data and codes that support the findings of this study presented in this study are available on request from the corresponding author. The data are not publicly available due to they form part of an ongoing study and privacy.

Acknowledgments: The authors would like to express their appreciation for the valuable suggestions and support of Fuyao Yang from State Key Laboratory of Advanced Power Transmission Technology, State Grid Smart Grid Research Institute Co., Ltd. and Peng Wu from State Grid Jiangsu Electric Power Co., Ltd. Research Institute.

Conflicts of Interest: Authors Bowei Zhang, Zhongqiu Zou, Xuebin Zhang, Wei Liu, and Hailin Su were employed by the company Anhui Red Magneto-electric Technology Co., Ltd.; Author Yu Han was employed by the company State Grid Smart Grid Research Institute Co., Ltd. The authors declare that the research was conducted in the absence of any commercial or financial relationships that could be construed as a potential conflict of interest.

References

1. Ni, J.L.; Hu, F.; Feng, S.J.; Kan, X.C.; Han, Y.Y.; Liu, X.S. Soft magnetic properties of FeSiAl/carbonyl iron composites with high magnetic permeability and low magnetic loss. *J. Alloys Compd.* **2021**, *887*, 161337. [CrossRef]
2. Zhou, L.; Yu, J.J.; Wang, Z.J.; Wang, H.B.; Huang, J.L.; Mu, W.Y.; Zheng, H.Q. Electromagnetic and microwave absorption properties of FeSiAl and flaky graphite filled Al_2O_3 composites with different FeSiAl particle size. *Ceram. Int.* **2020**, *46*, 4329–4334. [CrossRef]
3. Ni, J.L.; Duan, F.; Feng, S.J.; Hu, F.; Kan, X.C.; Liu, X.S. High performance of FeSiAl/hBN soft magnetic composites. *J. Alloys Compd.* **2022**, *897*, 163191. [CrossRef]
4. Yan, S.Q.; Dong, L.; Chen, Z.Y.; Wang, X.; Feng, Z.K. The effect of the microstructure on the DC-bias super position characteristic of NiCuZn ferrite. *J. Magn. Magn. Mater.* **2014**, *353*, 47–50. [CrossRef]
5. Legarra, E.; Apinaniz, E.; Plazaola, F.; Jimenez, J.A.; Pierna, A.R. Al versus Si competition in FeSiAl alloys. *J. Magn. Magn. Mater.* **2008**, *320*, e688–e691. [CrossRef]
6. Wei, Q.K.; Liu, B.Y.; Duan, S.X. Current ripple analysis and controller design for grid-connected converters considering the soft saturation nature of the powder cores. *IEEE Trans. Power Electron.* **2018**, *33*, 8827–8837. [CrossRef]
7. Wang, X.Y.; Lu, C.W.; Guo, F.; Lu, Z.C.; Li, D.R.; Zhou, S.X. New Fe-based amorphous compound powder cores with superior DC-bias properties and low loss characteristics. *J. Magn. Magn. Mater.* **2012**, *324*, 2727–2730. [CrossRef]
8. Ma, X.G.; Jiang, J.J.; Bie, S.W.; Miao, L.; Zhang, C.K.; Wang, Z.Y. Electronic structure and magnetism of $Fe_3Al_{1-x}Si_x$ alloys. *Intermetallics* **2010**, *18*, 2399–2403. [CrossRef]
9. Zhang, X.B.; Zeng, X.D.; Xue, L.; Cao, Z.; Liu, W.; Su, H.L.; Zou, Z.Q. Particle size selection principle of Fe-Si-Al SMCs for high-frequency and high-power applications. *J. Magn. Magn. Mater.* **2022**, *563*, 169803. [CrossRef]
10. Anhalt, M.; Weidenfeller, B.; Mattei, J.-L. Inner demagnetization factor in polymer-bonded soft magnetic composites. *J. Magn. Magn. Mater.* **2008**, *320*, e844–e848. [CrossRef]
11. Kronmuller, H. Theory of nucleation fields in inhomogeneous ferromagnets. *Phys. Stat. Sol. B* **1987**, *144*, 385–396. [CrossRef]
12. Anhalt, M. Systematic investigation of particle size dependence of magnetic properties in soft magnetic composites. *J. Magn. Magn. Mater.* **2008**, *320*, e366–e369. [CrossRef]
13. Guan, W.W.; Shi, X.Y.; Xu, T.T.; Wan, K.; Zhang, B.W.; Liu, W.; Su, H.L.; Zou, Z.Q.; Du, Y.W. Synthesis of well-insulated Fe-Si-Al soft magnetic composites via a silane-assisted organic/inorganic composite coating route. *J. Phys. Chem. Solids* **2021**, *150*, 109841. [CrossRef]
14. Zhang, Y.Q.; Chi, Q.; Liang, C.; Dong, Y.Q.; Cai, P.P.; Pan, Y.; Gong, M.J.; Huang, J.J.; Li, J.L.; He, A.N.; et al. Novel Fe-based amorphous compound powder cores with enhanced DC bias performance by adding FeCo alloy powder. *J. Magn. Magn. Mater.* **2020**, *507*, 166840. [CrossRef]
15. Liu, H.J.; Su, H.L.; Geng, W.B.; Sun, Z.G.; Song, T.T.; Tong, X.C.; Zou, Z.Q.; Wu, Y.C.; Du, Y.W. Effect of particle size distribution on the magnetic properties of Fe-Si-Al powder core. *J. Supercond. Nov. Magn.* **2016**, *29*, 463–468. [CrossRef]
16. Mei, C.; Xu, P.P.; Zhang, B.W.; Zhu, X.; Li, J.J.; Hu, F.; Su, H.L.; Liu, W.; Zou, Z.Q.; Wang, J.Z. Dependence of core loss on magnetization state under DC bias field for soft magnetic composites based on FeSiAl/FeSi powders. *J. Supercond. Nov. Magn.* **2023**, unpublished. [CrossRef]
17. Chang, C.T.; Guo, J.J.; Li, Q.; Zhou, S.M.; Liu, M.; Dong, Y.Q. Improvement of soft magnetic properties of FeSiBPNb amorphous powder cores by addition of FeSi powder. *J. Alloys Compd.* **2019**, *788*, 1177–1181. [CrossRef]
18. Dong, B.R.; Qin, W.; Su, Y.R.; Wang, X. Magnetic properties of FeSiCr@MgO soft magnetic composites prepared by magnesium acetate pyrolysis for high-frequency applications. *J. Magn. Magn. Mater.* **2021**, *539*, 168350. [CrossRef]
19. Liu, Z.H.; Dong, Y.Q.; Liu, X.C.; Lu, H.; Wu, Y.; Zhang, H.J.; He, A.N.; Li, J.W.; Wang, X.M. Microstructure and soft magnetic properties of $Fe_{85-x}Si_{9.6}Al_{5.4}Ti_x$ composite magnetic powder cores. *J. Alloys Compd.* **2021**, *885*, 160924. [CrossRef]
20. Xu, W.; Wu, C.; Yan, M. Preparation of Fe–Si–Ni soft magnetic composites with excellent high frequency properties. *J. Magn. Magn. Mater.* **2015**, *381*, 116–119. [CrossRef]
21. Huang, M.Q.; Wu, C.; Jiang, Y.Z.; Yan, M. Evolution of phosphate coatings during high-temperature annealing and its influence on the Fe and FeSiAl soft magnetic composites. *J. Alloys Compd.* **2015**, *644*, 124–130. [CrossRef]
22. Li, W.C.; Cai, H.W.; Kang, Y.; Ying, Y.; Yu, J.; Zheng, J.W.; Qiao, L.; Jiang, Y.; Che, S.L. High permeability and low loss bioinspired softmagnetic composites with nacre-like structure for high frequency applications. *Acta Mater.* **2019**, *167*, 267–274. [CrossRef]
23. Zhu, S.J.; Duan, F.; Feng, S.J.; Liu, X.S.; Kan, X.C.; Lv, Q.R.; Sun, W. Efficient inorganic-coated FeSiAl/WS_2 soft magnetic composites with low magnetic loss. *J. Alloys Compd.* **2023**, *936*, 168190. [CrossRef]
24. Li, Z.; Li, Z.Z.; Liu, X.Y.; Shi, S.Y.; Li, H.X.; Liu, X.G. Ultra-low core loss FeSiAl-based soft magnetic composites with ultra-thin MoO_3 composite insulating layer. *Ceram. Int.* **2022**, *48*, 29705–29714. [CrossRef]
25. Ni, J.L.; Zhu, S.J.; Feng, S.J.; Kan, X.C.; Liu, X.S. Investigation on magnetic properties of FeSiAl/$SrFe_{12}O_{19}$ composites. *J. Mater. Sci. Mater. Electron.* **2021**, *32*, 16956–16960. [CrossRef]

26. Lu, H.; Dong, Y.; Liu, X.; Liu, Z.; Wu, Y.; Zhang, H.J.; He, A.N.; Li, J.W.; Wang, X.M. Enhanced magnetic properties of FeSiAl soft magnetic composites prepared by utilizing PSA as resin insulating layer. *Polymers* **2021**, *13*, 1350. [CrossRef] [PubMed]
27. Zhou, L.; Xu, H.; Su, G.X.; Zhao, L.B.; Wang, H.B.; Wang, Z.J.; Li, Z. Tunable electromagnetic and broadband microwave absorption of SiO_2-coated FeSiAl absorbents. *J. Alloys Compd.* **2020**, *861*, 157966. [CrossRef]
28. O'Handley, R.C. *Modern Magnetic Materials Principles and Applications*; Wiley: New York, NY, USA, 2000; pp. 221–225.
29. Otani, Y.; Sasaki, S. Effects of the addition of silicon to 7075 aluminum alloy on microstructure, mechanical properties, and selective laser melting processability. *Mater. Sci. Eng. A* **2020**, *777*, 139079. [CrossRef]
30. Amin, N.A.A.M.; Shnawah, D.A.; Said, S.M.; Sabri, M.F.M.; Arof, H. Effect of Ag content and the minor alloying element Fe on the electrical resistivity of Sn-Ag-Cu solder alloy. *J. Alloys Compd.* **2014**, *599*, 114–120. [CrossRef]
31. Beguin, A.; Fabian, K. Demagnetization energy and internal stress in magnetite from temperature-dependent hysteresis measurements. *Geophys. Res. Lett.* **2021**, *48*, e2021GL096147. [CrossRef]
32. Xu, T.T.; Zhang, B.W.; Shi, Z.; Guan, W.W.; Wan, K.; Shi, X.Y.; Liu, W.; Su, H.L.; Zou, Z.Q.; Du, Y.W. Loss-separation study on silica-insulated gas-atomized Fe-Si-Al soft magnetic composites. *J. Magn.* **2020**, *25*, 223–228. [CrossRef]
33. Shokrollahi, H.; Janghorban, K. Soft magnetic composite materials (SMCs). *J. Mater. Process. Technol.* **2007**, *189*, 1–12. [CrossRef]
34. Fuzer, J.; Streckova, M.; Dobak, S.; Dakova, L.; Kollar, P.; Faberova, M.; Bures, R.; Osadchuk, Y.; Kurek, P.; Vojtko, M. Innovative ferrite nanofibres reinforced soft magnetic composite with enhanced electrical resistivity. *J. Alloys Compd.* **2018**, *753*, 219–227. [CrossRef]
35. Luo, F.; Fan, X.A.; Luo, Z.G.; Hu, W.T.; Wang, J.; Wu, Z.Y.; Li, G.Q.; Li, Y.W.; Liu, X. Preparation and magnetic properties of FeSiAl-based soft magnetic composites with MnO/Al_2O_3 insulation layer. *J. Magn. Magn. Mater.* **2020**, *498*, 166084. [CrossRef]